Electronic Supplementary Material (ESI) for Physical Chemistry Chemical Physics.

Supplementary material

Single-gas and mixed-gas permeation of N_2/CH_4 in thermally-rearranged TR-PBO membranes and their 6FDA-bisAPAF polyimide precursor studied by molecular dynamics simulations

Ioannis Tanis[1*], David Brown[1*], Sylvie Neyertz[1], Milind Vaidya[2], Jean-Pierre Ballaguet[2], Sebastien Duval[2], Ahmad Bahamdan[2]

[1] Univ. Grenoble Alpes, Univ. Savoie Mont Blanc, CNRS, Grenoble INP[#], LEPMI, 38000 Grenoble, France

[2] Saudi Aramco, Research & Development Center, P.O. Box 62, Dhahran 31311, Saudi Arabia

* Corresponding authors: ioannis.tanis77@gmail.com, David.Brown@univ-smb.fr

1. Force-field parameters

The following tables provide the TRIPOS 5.2 atom types [1] as well as the partial charges in all polyimide models. The latter were calculated on small sub-structures of both the precursor and the TR-PBO using *Gaussian* at the B3LYP/6-31G** level [2].

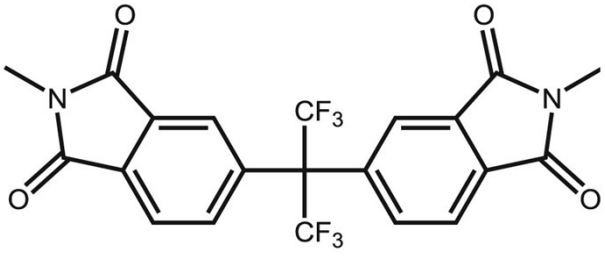

Figure S1: 6FDA fragment

	Charge/ e	Atom type	Element Symbol
1	0.2431	8	C(Car2)
2	0.1468	8	C(Car2)
3	-0.2963	8	C(Car2)
4	0.2399	8	C(Car2)
5	-0.1189	8	C(Car2)
6	-0.2888	8	C(Car2)
7	-0.3837	9	C(C2)
8	0.4027	10	C(CF2)
9	0.4027	10	C(CF2)
10	0.2399	8	$C(C_{ar2})$
11	-0.2963	8	$C(C_{ar2})$
12	-0.0138	8	$C(C_{ar2})$
13	0.2431	8	$C(C_{ar2})$
14	-0.1766	8	$C(C_{ar2})$
15	-0.2499	8	$C(C_{ar2})$
16	-0.1172	11	$F(F_2)$
17	-0.1172	11	$F(F_2)$
18	-0.1172	11	$F(F_2)$
19	-0.1172	11	$F(F_2)$
20	-0.1172	11	$F(F_2)$
21	-0.1172	11	$F(F_2)$
22	0.1816	13	H
23	0.1582	13	H
24	0.1638	13	H
25	0.1816	13	H
26	0.1638	13	H
27	0.1582	13	H
28	-0.4975	16	O(O3_bisA)
29	0.4043	13	H
30	-0.4975	16	O(O3_bisA)
31	0.4043	13	H

Table S1: Partial charges of 6FDA fragment

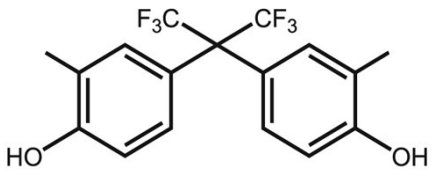

Figure S2: bisAPAF fragment

	Charge/ e	Atom type	Element Symbol
1	-0.5059	1	$C(C_1)$
2	0.4335	2	$C(C_{F1})$
3	0.4335	2	$C(C_{F1})$
4	-0.1148	7	$F(F_1)$
5	-0.1148	7	$F(F_1)$
6	-0.1148	7	$F(F_1)$
7	-0.1148	7	$F(F_1)$
8	-0.1148	7	$F(F_1)$
9	-0.1148	7	$F(F_1)$
10	0.2659	3	$C(C_{ar1})$
11	-0.1440	3	$C(C_{ar1})$
12	-0.0888	3	$C(C_{ar1})$
13	-0.1177	3	$C(C_{ar1})$
14	-0.0785	3	$C(C_{ar1})$
15	-0.1609	3	$C(C_{ar1})$
16	0.1323	13	H
17	0.1363	13	H
18	0.1425	13	H
19	0.2659	3	$C(C_{ar1})$
20	-0.1440	3	$C(C_{ar1})$
21	-0.0888	3	$C(C_{ar1})$
22	-0.1177	3	$C(C_{ar1})$
23	-0.0785	3	$C(C_{ar1})$
24	-0.1609	3	$C(C_{ar1})$
25	0.1323	13	H
26	0.1363	13	H
27	0.1425	13	H
28	0.5153	4	$C(C_{ket})$
29	0.5153	4	$C(C_{ket})$
30	-0.4426	5	$O(O_{ket})$
31	-0.4426	5	$O(O_{ket})$
32	-0.1744	6	$N(N_{am})$
33	0.5153	4	$C(C_{ket})$
34	0.5153	4	$C(C_{ket})$
35	-0.4426	5	$O(O_{ket})$
36	-0.4426	5	$O(O_{ket})$
37	-0.1744	6	$N(N_{am})$

Table S2: Partial charges of bisAPAF fragment.

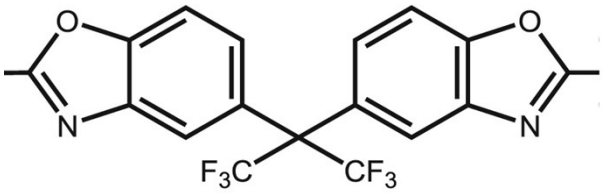

Figure S3: TR-PBO fragment.

	Charge/e	Atom type	Element Symbol
1	0.2743	8	$C(C_{ar2})$
2	0.2090	8	$C(C_{ar2})$
3	-0.2197	8	$C(C_{ar2})$
4	-0.0579	8	$C(C_{ar2})$
5	-0.1078	8	$C(C_{ar2})$
6	-0.2760	8	$C(C_{ar2})$
7	-0.0416	9	$C(C_2)$
8	0.4466	10	$C(C_{F2})$
9	0.4466	10	$C(C_{F2})$
10	-0.0579	8	$C(C_{ar2})$
11	-0.2197	8	$C(C_{ar2})$
12	0.2743	8	$C(C_{ar2})$
13	0.2090	8	$C(C_{ar2})$
14	-0.2760	8	$C(C_{ar2})$
15	-0.1078	8	$C(C_{ar2})$
16	-0.5331	6	$C(N_{am})$
17	0.4969	19	$C(C_{artr})$
18	-0.2753	18	$C(O_{tr})$
19	-0.5331	6	$N(N_{am})$
20	0.4969	19	$C(C_{artr})$
21	-0.2753	18	$O(O_{tr})$
22	-0.1448	11	$F(F_2)$
23	-0.1448	11	$F(F_2)$
24	-0.1448	11	$F(F_2)$
25	-0.1448	11	$F(F_2)$
26	-0.1448	11	$F(F_2)$
27	-0.1448	11	$F(F_2)$
28	0.1760	13	H
29	0.1801	13	H
30	0.1760	13	H
31	0.1801	13	H
32	0.1414	13	H
33	0.1414	13	H

Table S3: Partial charges of TR-PBO fragment.

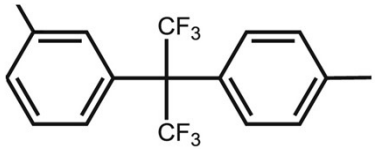

Figure S4: TR-PBO diamine *meta-para-* or *para-meta*-linked fragment.

	Charge/e	**Atom type**	**Element Symbol**
1	-0.0857	3	$C(C_{ar1})$
2	-0.1384	3	$C(C_{ar1})$
3	-0.0245	3	$C(C_{ar1})$
4	0.1489	3	$C(C_{ar1})$
5	-0.1487	3	$C(C_{ar1})$
6	-0.1154	3	$C(C_{ar1})$
7	-0.4015	1	$C(C_1)$
8	0.4374	2	$C(C_{F1})$
9	0.4374	2	$C(C_{F1})$
10	0.2138	3	$C(C_{ar1})$
11	-0.1635	3	$C(C_{ar1})$
12	-0.0860	3	$C(C_{ar1})$
13	-0.0855	3	$C(C_{ar1})$
14	-0.0860	3	$C(C_{ar1})$
15	-0.1635	3	$C(C_{ar1})$
16	-0.1228	7	$F(F_1)$
17	-0.1228	7	$F(F_1)$
18	-0.1228	7	$F(F_1)$
19	-0.1228	7	$F(F_1)$
20	-0.1228	7	$F(F_1)$
21	-0.1228	7	$F(F_1)$
22	0.1232	13	H
23	0.0816	13	H
24	0.1358	13	H
25	0.1321	13	H
26	0.1418	13	H
27	0.1232	13	H
28	0.1418	13	H
29	0.1199	13	H

Table S4: Partial charges of the *meta-para-* or *para-meta*-linked TR-PBO diamine fragment.

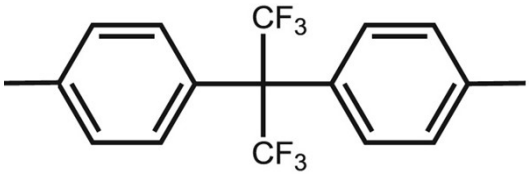

Figure S5: TR-PBO diamine *para-para*-linked fragment

	Charge /e	**Atom type**	**Element Symbol**
1	-0.1554	3	$C(C_{ar1})$
2	-0.0687	3	$C(C_{ar1})$
3	-0.1438	3	$C(C_{ar1})$
4	0.1500	3	$C(C_{ar1})$
5	-0.1438	3	$C(C_{ar1})$
6	-0.0687	3	$C(C_{ar1})$
7	0.1406	13	H
8	-0.2620	1	$C(C_1)$
9	0.3447	2	$C(C_{F1})$
10	0.3447	2	$C(C_{F1})$
11	0.1500	3	$C(C_{ar1})$
12	-0.1438	3	$C(C_{ar1})$
13	-0.0687	3	$C(C_{ar1})$
14	-0.1554	3	$C(C_{ar1})$
15	-0.0687	3	$C(C_{ar1})$
16	-0.1438	3	$C(C_{ar1})$
17	-0.1150	7	$F(F_1)$
18	-0.1150	7	$F(F_1)$
19	-0.1150	7	$F(F_1)$
20	-0.1150	7	$F(F_1)$
21	-0.1150	7	$F(F_1)$
22	-0.1150	7	$F(F_1)$
23	0.1406	13	H
24	0.1406	13	H
25	0.1406	13	H
26	0.1406	13	H
27	0.1406	13	H
28	0.1406	13	H
29	0.1406	13	H

Table S5: Partial charges of *para-para*-linked TR-PBO diamine fragment.

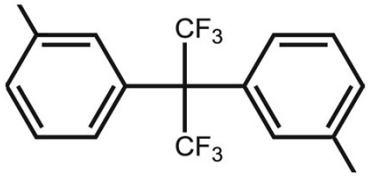

Figure S6: TR-PBO diamine *meta-meta*-linked fragment

	Charge/e	Atom type	Element Symbol
1	-0.0822	3	C(Car1)
2	-0.1038	3	C(Car1)
3	0.0035	3	C(Car1)
4	0.1020	3	C(Car1)
5	-0.1182	3	C(Car1)
6	-0.1513	3	C(Car1)
7	-0.3696	1	C(C1)
8	0.4598	2	(C_{F1})
9	0.4598	2	(C_{F1})
10	0.1020	3	C(Car1)
11	0.0035	3	C(Car1)
12	-0.1038	3	C(Car1)
13	-0.0822	3	C(Car1)
14	-0.1513	3	C(Car1)
15	-0.1182	3	C(Car1)
16	-0.1275	7	F(F_1)
17	-0.1275	7	F(F_1)
18	-0.1275	7	F(F_1)
19	-0.1275	7	F(F_1)
20	-0.1275	7	F(F_1)
21	-0.1275	7	F(F_1)
22	0.0707	13	H
23	0.1341	13	H
24	0.1354	13	H
25	0.0707	13	H
26	0.1354	13	H
27	0.1341	13	H
28	0.1180	13	H
29	0.1180	13	H

Table S6: Partial charges of *meta-meta*-linked TR-PBO fragment.

2. Effect of the cooling rate on the relaxed density at room temperature

Cooling rates in MD are always many orders of magnitude higher than those used in experiments and they can affect some properties. Figure S7 provides a comparison of the "classical cooling rate" used in MD (-1 K/ps) to a faster one (-10 K/ps) and to a shorter one (-0.1 K/ps). As expected [3-5], the three values slightly differ but they all remain close to the target experimental value of 1535 kg m^{-3} (pink line) [6,7].

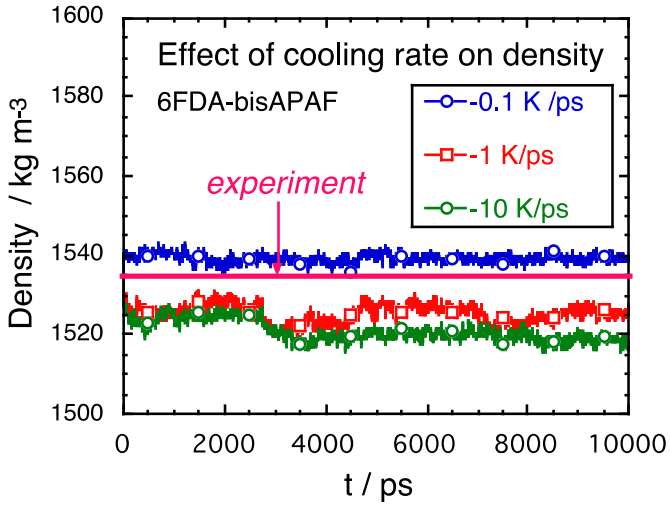

Figure S7: Relaxation of the density for the pure 6FDA-bisAPAF model using three different cooling rates available to MD simulations, *i.e.* -0.1 K/ps, -1 K/ps and -10 K/ps. The pink line is the experimental density measured by Han *et al.* [6].

3. Energies and densities relaxations

Figure S8 provides evidence that the 4000 ps duration of most MD simulations carried out in this work is sufficient to equilibrate both the total potential energy and the density.

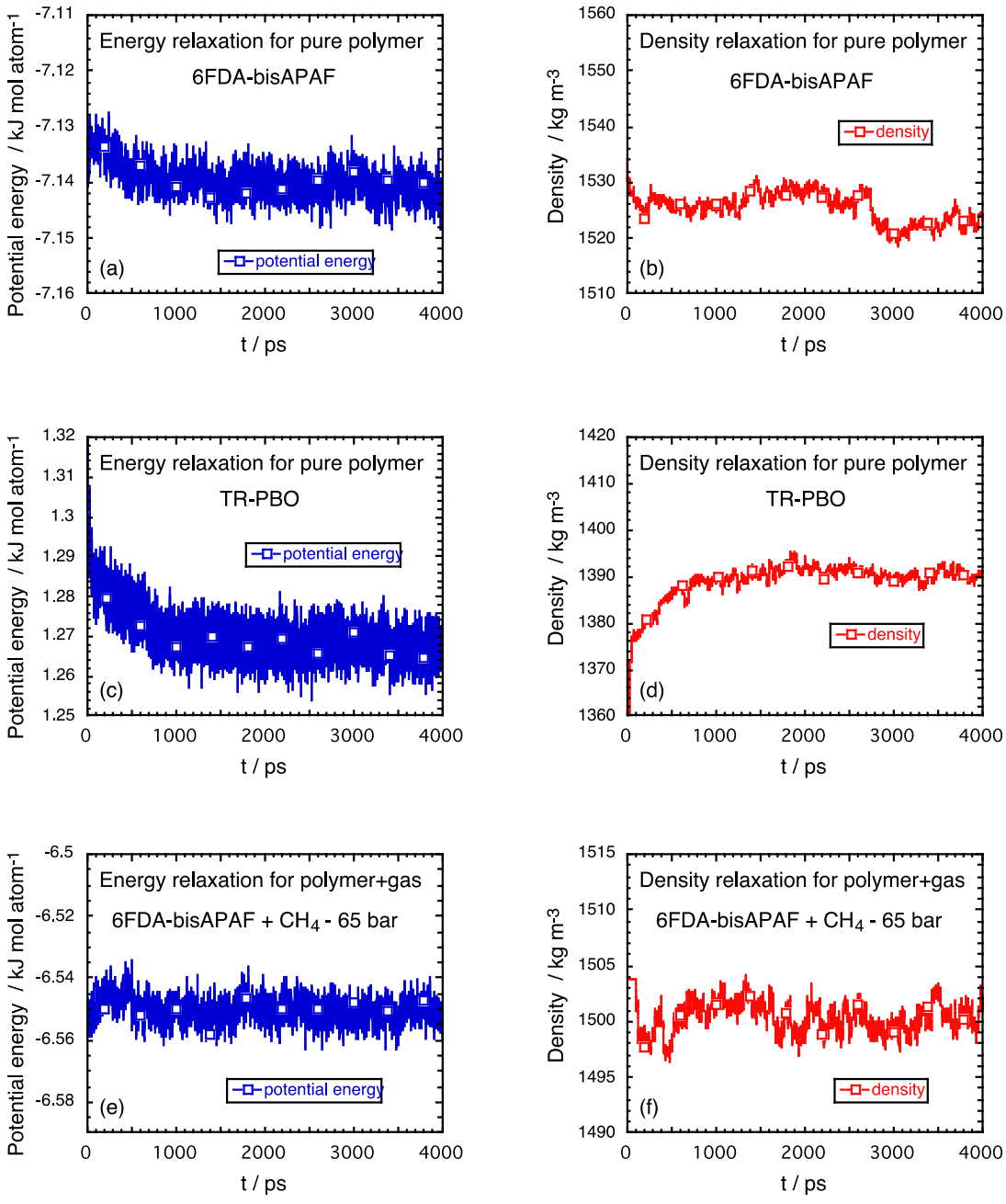

Figure S8: Relaxation of the total potential energy and the density for several systems over the 4000 ps timescale used for most of the MD production runs (pure polymers and gas sorptions phases). The properties were usually averaged over the last 2000 ps.

4. Effect of penetrant concentration on chain configurations

To illustrate the effects of the penetrants on the local structure and segmental dynamics, Figure S9 reports (a) the mean square end-to-end distances $\langle R^2 \rangle$ and (b) the mean square radii of gyration $\langle S^2 \rangle$ of the 6FDA-bisAPAF precursor loaded with methane. The error bars are the standard deviations.

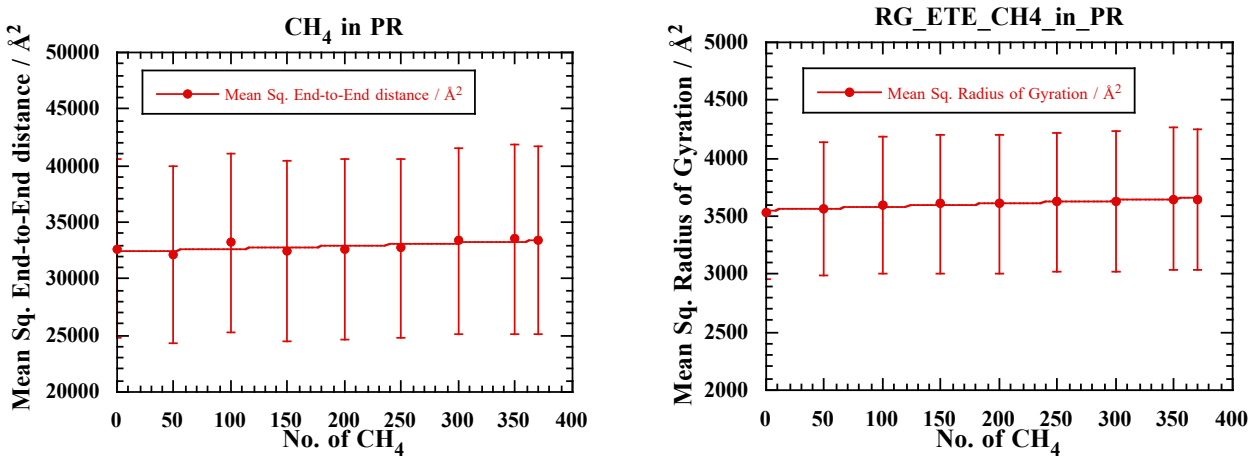

(a) **(b)**

Figure S9: **(a)** Mean square end-to-end distance and **(b)** mean square radius of gyration of the precursor polyimide as a function of the number of methane penetrants.

Although there is a slight tendency to increase the mean square end-to-end distance and the mean square radius of gyration, the error bars due to the small number of chains are too large to ascribe this tendency to a concentration effect. The increasing trends in chain dimensions are thus consistent with the limited volume swelling but there are no large configurational changes.

References

1. M. Clark, R. D. Cramer and N. Van Opdenbosch, *Journal of Computational Chemistry*, 1989, **10**, 982-1012.
2. M. J. Frisch, G. W. Trucks, H. B. Schlegel, G. E. Scuseria, M. A. Robb, J. R. Cheeseman, G. Scalmani, V. Barone, B. Mennucci, G. A. Petersson, H. Nakatsuji, M. Caricato, X. Li, H. P. Hratchian, A. F. Izmaylov, J. Bloino, G. Zheng, J. L. Sonnenberg, M. Hada, M. Ehara, K. Toyota, R. Fukuda, J. Hasegawa, M. Ishida, T. Nakajima, Y. Honda, O. Kitao, H. Nakai, T. Vreven, J. A. Montgomery Jr., J. E. Peralta, F. Ogliaro, M. Bearpark, J. J. Heyd, E. Brothers, K. N. Kudin, V. N. Staroverov, R. Kobayashi, J. Normand, K. Raghavachari, A. Rendell, J. C. Burant, S. S. Iyengar, J. Tomasi, M. Cossi, N. Rega, J. M. Millam, M. Klene, J. E. Knox, J. B. Cross, V. Bakken, C. Adamo, J. Jaramillo, R. Gomperts, R. E. Stratmann, O. Yazyev, A. J. Austin, R. Cammi, C. Pomelli, J. W. Ochterski, R. L. Martin, K. Morokuma, V. G. Zakrzewski, G. A. Voth, P. Salvador, J. J. Dannenberg, S. Dapprich, A. D. Daniels, O. Farkas, J. B. Foresman, J. V. Ortiz, J. Cioslowski and D. J. Fox, *Gaussian 09, Revision A.02*, 2009.
3. S. G. Falkovich, S. V. Lyulin, V. M. Nazarychev, S. V. Larin, A. A. Gurtovenko, N. V. Lukasheva and A. V. Lyulin, *J. Polym. Sci., Part B: Polym. Phys.*, 2014, **52**, 640-646.
4. S. V. Lyulin, S. V. Larin, A. A. Gurtovenko, V. M. Nazarychev, S. G. Falkovich, V. E. Yudin, V. M. Svetlichnyi, I. V. Gofman and A. V. Lyulin, *Soft Matter*, 2014, **10**, 1224-1232.
5. V. M. Nazarychev, A. V. Lyulin, S. V. Larin, A. A. Gurtovenko, J. M. Kenny and S. V. Lyulin, *Soft Matter*, 2016, **12**, 3972-3981.
6. S. H. Han, N. Misdan, S. Kim, C. M. Doherty, A. J. Hill and Y. M. Lee, *Macromolecules*, 2010, **43**, 7657-7667.
7. Y. Jiang, F. T. Willmore, D. Sanders, Z. P. Smith, C. P. Ribeiro, C. M. Doherty, A. Thornton, A. J. Hill, B. D. Freeman and I. C. Sanchez, *Polymer*, 2011, **52**, 2244-2254.